

ANALYSIS OF UPSCALING ABSOLUTE PERMEABILITY

X.H. WU¹

Applied & Computational Mathematics
California Institute of Technology
Pasadena, CA 91125

Y. EFENDIEV

Department of Mathematics
Texas A&M University
College Station, TX 77843

T.Y. HOU

Applied & Computational Mathematics
California Institute of Technology
Pasadena, CA 91125

ABSTRACT. Flow based upscaling of absolute permeability has become an important step in practical simulations of flow through heterogeneous formations. The central idea is to compute upscaled, grid-block permeability from fine scale solutions of the flow equation. Such solutions can be either local in each grid-block or global in the whole domain. It is well-known that the grid-block permeability may be strongly influenced by the boundary conditions imposed on the flow equations and the size of the grid-blocks. We show that the upscaling errors due to both effects manifest as the resonance between the small physical scales of the media and the artificial size of the grid blocks. To obtain precise error estimates, we study the scale-up of single phase steady flows through media with periodic small scale heterogeneity. As demonstrated by our numerical experiments, these estimates are also useful for understanding the upscaling of general random media. It is further shown that the over-sampling technique introduced in our previous work can be used to reduce the resonance error and obtain boundary-condition independent, grid-block permeability. Some misunderstandings in scale up studies are also clarified in this work.

1. Introduction. The direct numerical simulation of flows through porous formations is difficult due to the fine scale heterogeneity in the media and also the complexity of the dynamic systems (see e.g., [11, 25, 22] for recent developments). An accurate well-resolved computation often requires tremendous amount of computer memory and CPU time which can easily exceed the limit of today's computer resources. On the other hand, in practice, it is often sufficient to predict the large scale solutions to certain accuracy. Therefore, alternative approaches have been developed.

1991 *Mathematics Subject Classification.* Primary 65F10, 65F30.

Key words and phrases. Upscaling, Homogenization, Resonance, Over-sampling.

¹Current address: ExxonMobil Upstream Research Company, P. O. Box 2189, Houston TX 77252.

A common approach is to “scale up” a heterogeneous medium. For a single phase flow problem, the medium is solely described by the permeability field which can be very oscillatory. The goal of upscaling is to find an effective representation of the permeability on a coarse mesh so that the large scale flow can be correctly computed on this mesh. The computational cost is thus greatly reduced. The main result of upscaling is often the block permeability, a constant tensor computed in each grid block. Both analytical and numerical methods have been used in upscaling, see [23] and [19] for recent extensive reviews. While various formulations are proposed based on different physical and numerical considerations, we only consider flow based upscaling in this paper. The central theme is to compute the block permeability from certain averages of fine scale flow solutions. These fine scale flows can be obtained from either the global solutions of the flow equation in the whole reservoir [26] or the local solutions in each grid block. The latter approach, though, demands much less computing power. For convenience, we refer to the two approaches as *global* and *local* Laplacian, respectively.

Recently, the local Laplacian method has been extensively studied and successfully used in practical computations (see, e.g., the above review articles). However, some important issues associated with the method have not been addressed satisfactorily. For example, ideally the block permeability should only depend on the structure and the partition of the medium [15]. But in practice it has been observed that the block permeability can be strongly affected by the boundary conditions imposed for the local flow equation (cf. [5]). Furthermore, it is well-known that when the size of grid blocks is close to the scale of heterogeneity, the pressure and flow solutions computed on such a grid can have large error. The understanding of these questions is indeed crucial for a quantification of the upscaling error.

Here we provide a rigorous analysis of the upscaling error. We assume that the underlying medium is periodic at small scales, however the upscaling formulations we analyze are fully general. The periodic assumption enables us to explore the detail structures of the local fine scale solutions using the homogenization theory [2]; therefore accurate *a priori* estimates can be obtained. We show that the upscaling error appears as a *resonance* between the small physical scales of the medium and the artificial mesh scale (size). Indeed the error is given by the ratio between the two scales; it increases as the size of grid blocks gets close to the small physical scales. We also show that the effect of different boundary conditions lies in a narrow region near the boundaries of grid blocks and it contributes to part of the resonance error. Therefore, by using an *over-sampling* technique [12], we can reduce the boundary layer effect and obtain upscaled grid-block permeability *independent* of the boundary conditions. In this case, the scale-up accuracy is also improved. We provide numerical experiments to demonstrate these analytical findings. The upscaling of general heterogeneous media is much more difficult to analyze. However, the insights obtained through analyzing the model problem are useful in understanding the upscaling error in problems with more general random media. This is demonstrated through numerical tests.

The analysis here is motivated by the recent development of a multiscale finite element method for solving porous media flows [14, 12]. In this method, the permeability is not explicitly upscaled; the focus is on the final solutions: the pressure and velocity on the coarse grids. Similar resonance error was found [14]. The problem is further studied in more detail in [8]. Although the mechanisms of resonance are the same, the effect of resonance is stronger for the upscaling methods analyzed here (see Section 3).

The rest of the paper is organized as follows. In Section 2, we present a coherent account of upscaling formulations. Different formulations are shown to be equivalent under proper conditions. Section 3 starts with a brief review of the homogenization theory for media with periodic small scales. The analysis of resonance error is given subsequently. In Section 4 we discuss the use of over-sampling technique in upscaling. Numerical results are given in the last section.

2. Formulations.

2.1. Effective and grid-block permeability. Consider single phase Darcy's flows in a medium Ω :

$$\mathbf{u}^\epsilon = -K^\epsilon(\mathbf{x})\nabla p^\epsilon, \quad \nabla \cdot \mathbf{u}^\epsilon = f; \quad (1)$$

where \mathbf{u} is the velocity, K is the permeability tensor which is symmetric and positive definite (assuming unit viscosity), p is the pressure, and f is the source. Note that ϵ is a small parameter indicating the length of the small scales. To solve (1) numerically, one need to cover Ω with a mesh consisting of finite number of grid blocks. An accurate solution is obtained if $h \ll \epsilon$ (h being the size of grid blocks). This requirement is often too restrictive for practical simulations due to large disparity of length scales.

The ultimate goal of upscaling is to compute solutions on a mesh with mesh size $h \geq \epsilon$. The approach considered in this paper is to replace $K^\epsilon(\mathbf{x})$ with the grid-block permeabilities, \tilde{K} , a constant tensor defined in each grid block. By definition, \tilde{K} is a *discrete* quantity relying on the discretization of the medium. In particular, \tilde{K} depends on the location and geometry of the grid block in which it is computed. The essential requirements for \tilde{K} is that it leads to pressure and velocity solutions with desired accuracy. Moreover, one hopes that \tilde{K} depends *only* on the heterogeneous permeability field and the discretization of the medium, so that it can be used in different flow scenarios once it is computed.

Different definitions of \tilde{K} have been proposed (cf. [23]). Following [20], we define \tilde{K} in a given grid block V such that

$$\tilde{K} \langle \nabla p^\epsilon \rangle_V = -\langle \mathbf{u}^\epsilon \rangle_V, \quad (2)$$

where p^ϵ and \mathbf{u}^ϵ are solutions of (1) in V (with appropriate boundary conditions, see Section 2.2), and

$$\langle \cdot \rangle_V = \frac{1}{V} \int_V (\cdot) d\mathbf{x}$$

is the volume average over V . In 3-D, three pressure solutions are sufficient in order to determine \tilde{K} from (2), provided that the volume averages of the pressure gradients are linearly independent. It is evident that different sets of pressure solutions in general lead to different \tilde{K} s. This makes it difficult to analyze the use of \tilde{K} in more general flow simulations. It seems that an analysis of upscaling error is feasible only if \tilde{K} can be related to an intrinsic property of the medium. Such an intrinsic property is the effective permeability of the medium, K^* .

For general heterogeneous media, the existence of K^* is an open question. Physically, K^* exists when there exists an elementary representative volume (REV) such that the averages of the pressure gradient and velocity over this volume have a unique well-defined relation. An REV should be sufficiently large to contain enough small scale information for a meaningful average and yet sufficiently small to reflect the large scale heterogeneity of the medium [1]. These ideas are expressed more

rigorously in the homogenization theory. Mathematically, K^* is defined through the following criteria [2]: for any measurable $V \subset \Omega$,

$$\lim_{\epsilon \rightarrow 0} \langle \nabla p^\epsilon \rangle_V = \langle \nabla p \rangle_V, \quad \lim_{\epsilon \rightarrow 0} \langle \mathbf{u}^\epsilon \rangle_V = \langle \mathbf{u} \rangle_V, \quad (3)$$

where p and \mathbf{u} are the solutions of the effective (or homogenized) equation

$$\mathbf{u} = -K^*(\mathbf{x})\nabla p, \quad \nabla \cdot \mathbf{u} = f \quad (4)$$

in Ω . In (3), we have replaced the weak convergence of ∇p^ϵ and \mathbf{u}^ϵ by their equivalent definitions (cf. [9]). It can further be shown that the sufficient conditions for the existence of K^* , p , and \mathbf{u} is that for any V the limits on the left-hand sides of (3) exist (see [16] for more rigorous details). This condition is very general; it does not assume any structure of the small scales of K^* .

The nice property of K^* (when it exists) are [16]: (1) it is unique; (2) it is independent of the source term f and of the boundary condition on $\partial\Omega$; and (3) it can be determined locally, i.e., to determine K^* at a point $\mathbf{x} \in \Omega$, one needs only to consider (1) in the neighborhoods of \mathbf{x} . This last property of K^* is the foundation of all local Laplacian methods.

It is easy to see that \tilde{K} is an approximation of K^* . More specifically, consider a point $\mathbf{x} \in \Omega$ and grid block $V \in \Omega$ containing \mathbf{x} . From (2), (3) and (4), we have

$$\begin{aligned} \langle \mathbf{u}^\epsilon \rangle_V &\approx \lim_{\epsilon \rightarrow 0} \langle \mathbf{u}^\epsilon \rangle_V = -\langle K^*\nabla p \rangle_V \approx -K^*(\mathbf{x})\nabla p, \\ \langle \nabla p^\epsilon \rangle_V &\approx \lim_{\epsilon \rightarrow 0} \langle \nabla p^\epsilon \rangle_V = \langle \nabla p \rangle_V. \end{aligned}$$

Thus, $\tilde{K} \approx K^*(\mathbf{x})$. In Section 3 we analyze the accuracy of this approximation in details. Then we analyze the difference between the upscaled solution and the homogenized solution of (4) and hence, indirectly, the difference between the upscaled solution and the fine scale solution of (1).

2.2. Local Laplacian formulations. In these methods, \tilde{K} is determined from the local flow solutions in the grid blocks. The main differences among various formulations are the boundary conditions imposed on the flow equation and the averaging processes for computing \tilde{K} . Here we provide a unified view of the local Laplacian approach and clarify some misconceptions.

Consider a cubic grid block V of size h in a d -dimensional space (see Fig. 1). To determine \tilde{K} from (2), we need d sets of fine scale flow solutions in V , \mathbf{u}_i^ϵ and p_i^ϵ ($i = 1, \dots, d$), such that $\langle \nabla p_i^\epsilon \rangle_V$ are linearly independent. These fine scale solutions are solved from

$$\mathbf{u}_i^\epsilon = -K^\epsilon \nabla p_i^\epsilon, \quad \nabla \cdot \mathbf{u}_i^\epsilon = 0 \quad (5)$$

in the grid block V . Note that the source term is set to zero because of the second property of K^* mentioned above. Eq. (5) is well posed with suitable boundary conditions on ∂V . Define $w_i^\epsilon = p_i^\epsilon - x_i$. Then

$$\mathbf{u}_i^\epsilon = -K^\epsilon (\nabla w_i^\epsilon + \mathbf{e}_i), \quad (6)$$

\mathbf{e}_i being the unit vector in the i th direction. Thus, the linear pressure drop condition [10], the periodic boundary condition [21, 17, 5], and the widely used pressure-drop no-flow condition can then be formulated respectively as

$$w_i^\epsilon = 0 \quad \text{on } \partial V; \quad (7)$$

$$w_i^\epsilon \text{ being periodic on } V; \quad (8)$$

$$w_i^\epsilon = 0 \text{ on } \Gamma_i, \quad \mathbf{n} \cdot \mathbf{u}_i^\epsilon = 0 \text{ on } \Gamma_j \ (j \neq i), \quad (9)$$

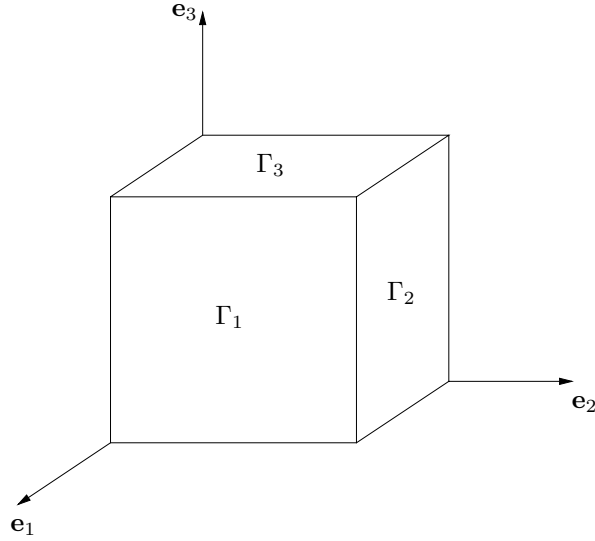


FIGURE 1. A 3D grid block.

where Γ^i are the faces of ∂V normal to \mathbf{e}_i . We note that (7) can be conveniently imposed on ∂V if V is not a rectangular box. (8) and (9) are not as flexible, but one can embed V in a larger rectangular box V' and solve (5) in V' . This strategy indeed has some advantages, see Section 4.

Conditions (7) and (8) guarantee the linear independence of the averages of pressure gradients. In fact, if either (7) or (8) holds, the Green's Theorem gives

$$\langle \nabla p_i^\epsilon \rangle_V = \mathbf{e}_i + \frac{1}{V} \int_{\partial V} w_i^\epsilon \mathbf{n} ds = \mathbf{e}_i. \quad (10)$$

Thus, (2) can be simplified as

$$\tilde{K} \mathbf{e}_i = -\langle \mathbf{u}_i^\epsilon \rangle_V. \quad (11)$$

Another nice property of (7) and (8) is that they lead to symmetric and positive definite \tilde{K} . Indeed, (10) and (11) yield

$$\mathbf{e}_i \cdot \tilde{K} \mathbf{e}_j = -\mathbf{e}_i \cdot \langle \mathbf{u}_j^\epsilon \rangle_V = -\langle (\nabla p_i^\epsilon - \nabla w_i^\epsilon) \cdot \mathbf{u}_j^\epsilon \rangle_V.$$

By (5), (7) (or (8)), and integration by parts,

$$\int_V \nabla w_i^\epsilon \cdot \mathbf{u}_j^\epsilon d\mathbf{x} = \int_{\partial V} w_i^\epsilon \mathbf{n} \cdot \mathbf{u}_j^\epsilon ds = 0. \quad (12)$$

Therefore,

$$\mathbf{e}_i \cdot \tilde{K} \mathbf{e}_j = \langle \nabla p_i^\epsilon \cdot K^\epsilon \nabla p_j^\epsilon \rangle_V, \quad (13)$$

hence \tilde{K} is symmetric and positive definite. Eq. (13) gives us another way to compute \tilde{K} . In fact, it gives symmetry up to the round off error in numerical computations.

In contrast to (7) and (8), the condition (9) does not enjoy the above properties. Because of (9), in general (10) is invalid. Indeed, we have

$$\int_{\partial V} w_i^\epsilon \mathbf{n} ds = \sum_{j \neq i} C_j \mathbf{e}_j \neq 0,$$

C_j being some constants. Thus, $\langle \nabla p_i^\epsilon \rangle_V$ is not aligned with \mathbf{e}_i . Consequently, (11) and (13) are invalid under the boundary condition (9). In this case, the original equation (2) should be used. Without (10), it is more difficult to show the linear independence of $\langle \nabla p_i^\epsilon \rangle_V$. In Section 4 using numerical examples we show that (9) works as well as (7) and (8).

There are many other choices of boundary conditions, here we only consider the ones listed above because they are simple and easy to use in practice. Some other simple boundary conditions may generate singularities in the local fine scale solutions which are difficult to analyze and compute, thus they should be avoided. An example is to let $p^\epsilon = 1$ on one face of ∂V and $p^\epsilon = 0$ on the other faces.

We remark that several popular upscaling formulations can be included in the above formulation based on (2) and (5). For example, with the periodic boundary condition (8), the formulations in [21, 5] are included. The block permeability Kitanidis [17] derived using the method of moments under the periodic boundary condition is identical to the symmetric part of \tilde{K} , which equals \tilde{K} itself. Moreover, the formulation based on the conservation of dissipation [15] is equivalent to the above formulations under the conditions (7) and (8) (see Appendix A).

2.3. Volume vs. surface averages. In many practical upscaling computations, instead of using the volume averaged flux on the right hand side of (2), people often average the velocity over the outflow surface. This approach seems appealing physically, but it may give incorrect results.

Durlofsky [5] noticed that under the periodic boundary condition (8), the volume average of velocity can be replaced by the averaged outflow. This is also true for the Dirichlet condition (7). Indeed, using (5), (13), and integration by parts we have

$$\tilde{K}_{ij} = \frac{1}{V} \int_{\partial V} p_i^\epsilon \mathbf{n} \cdot \mathbf{u}_j^\epsilon ds \quad (14)$$

By using (7) or (8), it can be further reduced to

$$\tilde{K}_{ij} = \frac{1}{\Gamma_i} \int_{\Gamma_i} \mathbf{e}_i \cdot \mathbf{u}_j^{\epsilon+} ds; \quad (15)$$

the plus sign indicates that the flux is taken at the outflow boundary. We see that the volume averaged flow is equivalent to the averaged outflow under the condition (7) or (8) for rectangular grid blocks. Furthermore, since \mathbf{u}_j^ϵ is divergence free, under (8) one can show that the averaged flux are identical over any cross section of V parallel to Γ_i . This property, however, is not shared by (7).

The boundary condition (7) (or (8)) is crucial in the derivation of (15) from (2). The derivation breaks down under the pressure-drop no-flow condition (9). As pointed out in the literature, only when \tilde{K} is diagonal can one obtain the accurate result using (9) together with (15). This can also be seen from the above derivation.

A common misunderstanding is that one cannot compute the off-diagonal entries of \tilde{K} if (9) is used. This conclusion is often deduced mistakenly by confusing the volume and surface averaged flows. Instead, under (9) the right-hand side of (15)

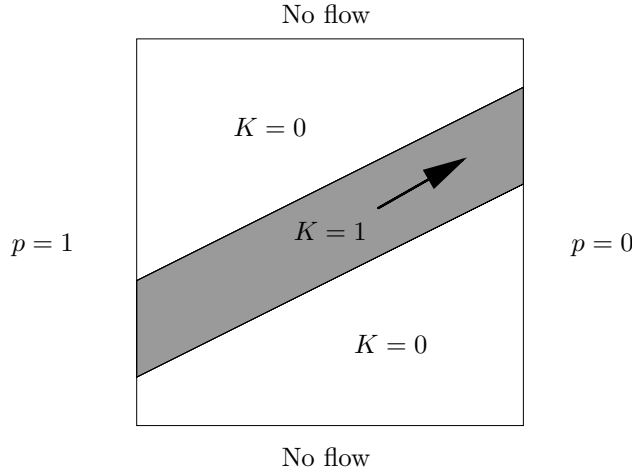


FIGURE 2. Flow through a channel. There is no flow through the top and bottom surfaces, but the volume averaged flow has a vertical component.

vanishes for $i \neq j$, but the right-hand side of (2) may be nonzero. A simple example is demonstrated in Fig. 2.3 (see also Section 5).

3. Accuracy of Upscaling. We now study the accuracy of the upscaling method given in the last section. We assume the medium is periodic at the small scale, i.e., K^ϵ has the form $K(\mathbf{x}, \mathbf{x}/\epsilon)$, where $K(\mathbf{x}, \mathbf{y})$ is periodic in the \mathbf{y} variable in a unit cube Y . For this type of media, the homogenization theory [2] makes it possible to understand the upscaling precisely. For simplicity, we assume that $K(\mathbf{x}, \mathbf{y})$ is smooth in both \mathbf{x} and \mathbf{y} below. For further analysis, we assume that K^ϵ is sufficiently smooth function, though it is sufficient to assume $K^\epsilon \in C^1$

In the following, unless otherwise stated, Einstein's summation convention is used, i.e., summation is taken over repeated indices; V is a cubic block of size h ; C denotes a generic constant independent of h and ϵ .

In the derivations below, we use the $L^2(V)$ based Sobolev spaces $H^k(V)$ equipped with norms and seminorms

$$\|u\|_{k,V} = \left(\int_V \sum_{|\alpha| \leq k} |D^\alpha u|^2 \right)^{\frac{1}{2}},$$

$$|u|_{k,V} = \left(\int_V \sum_{|\alpha|=k} |D^\alpha u|^2 \right)^{\frac{1}{2}}.$$

We use $\|\cdot\|_V = \|\cdot\|_{0,V}$ for the L^2 norm. $H_0^1(V)$ consists of those functions in $H^1(\Omega)$ that vanish on ∂V .

3.1. Review of homogenization theory. With K^ϵ given above, the homogenized effective permeability is given by [2]

$$K_{ij}^*(\mathbf{x}) = \langle (\mathbf{e}_i + \nabla_{\mathbf{y}}\chi^i(\mathbf{x}, \mathbf{y})) \cdot K(\mathbf{x}, \mathbf{y})(\mathbf{e}_j + \nabla_{\mathbf{y}}\chi^j(\mathbf{x}, \mathbf{y})) \rangle_Y, \quad (16)$$

where $\langle \cdot \rangle_Y = \int_Y (\cdot) d\mathbf{y} / Y$, $\nabla_{\mathbf{y}}$ is the gradient with respect to \mathbf{y} , and χ^j is the periodic solution of

$$\nabla_{\mathbf{y}} \cdot K(\mathbf{x}, \mathbf{y})[\nabla_{\mathbf{y}}\chi^j(\mathbf{x}, \mathbf{y}) + \mathbf{e}_j] = 0 \quad (17)$$

in Y and satisfies $\int_Y \chi^j d\mathbf{y} = 0$. Note that \mathbf{x} is just a parameter in the above equations. Since $K(\mathbf{x}, \mathbf{y})$ is smooth, it is easy to see that $K^*(\mathbf{x})$ is also smooth.

Assuming Dirichlet boundary condition: $p^\epsilon = g(\mathbf{x})$ on $\partial\Omega$, the solution of (1) has the following expansion [2]:

$$p^\epsilon(\mathbf{x}) = p(\mathbf{x}) + \epsilon p'(\mathbf{x}, \mathbf{y}) + \epsilon \theta^\epsilon + O(\epsilon^2). \quad (18)$$

Here $p(\mathbf{x})$ is the solution of the homogenized equation (4) with K^* given by (16) and boundary condition $p = g$ on $\partial\Omega$; p' is given by

$$p'(\mathbf{x}, \mathbf{y}) = \frac{\partial p}{\partial x_i}(\mathbf{x}) \chi^i(\mathbf{x}, \mathbf{y}),$$

and θ^ϵ satisfies

$$\nabla \cdot K^\epsilon \nabla \theta^\epsilon = 0 \quad \text{in } \Omega, \quad \theta^\epsilon = -p' \quad \text{on } \partial\Omega. \quad (19)$$

We note that the main role of θ^ϵ is to correct the discrepancy in the boundary conditions between p^ϵ and its first order expansion $p + \epsilon p'$. The discrepancy is caused by the fact that p' is periodic in \mathbf{y} and hence generally nonzero along $\partial\Omega$.

For convex polygonal domains, it can be shown that [18]

$$\|\nabla p^\epsilon - \nabla(p + \epsilon p' + \epsilon \theta^\epsilon)\|_\Omega \leq C\epsilon \|p\|_{2,\Omega}, \quad (20)$$

where $\|\cdot\|_\Omega$ and $\|\cdot\|_{2,\Omega}$ are the L_2 and H^2 norms over Ω (see Appendix B); C is a constant independent of ϵ and the size of Ω . Thus, the formal expansion (18) can be rigorously justified.

3.2. Estimates for upscaled permeability and solutions. Now consider the formulation for \tilde{K} given by (2) and (5) with boundary condition (7). Note that in this case (2) is equivalent to (13). Below, we use (13) instead of (2) in the analysis. With minor modifications, the following derivation also holds if the periodic boundary condition (8) is used. But the derivation is more complicated with (9) (note that (13) is invalid in this case). We outline the analysis here and leave some details in Appendix B. All estimates derived below are for $h \gg \epsilon$, which is often the case in scale-up. Our main result is the following estimate for the grid-block permeability:

$$\left| \tilde{K}_{ij} - \langle K_{ij}^*(\mathbf{x}) \rangle_V \right| \leq C_1 \frac{\epsilon}{h} + C_2 h + C_3 \epsilon. \quad (21)$$

Since $K^*(\mathbf{x})$ is smooth, $|K_{ij}^*(\mathbf{x}) - \langle K_{ij}^* \rangle_V| = O(h)$, thus (21) still holds if we replace $\langle K_{ij}^* \rangle_V$ by $K_{ij}^*(\mathbf{x})$ with $\mathbf{x} \in V$.

To simplify the presentation, it is convenient to introduce a vector $\boldsymbol{\chi} = (\chi^i)$ ($i = 1, \dots, d$). Define tensor $E(\mathbf{x}, \mathbf{y}) = I + \nabla_{\mathbf{y}}\boldsymbol{\chi}(\mathbf{x}, \mathbf{y})$. Eqs. (16) and (17) can be written as

$$K^*(\mathbf{x}) = \langle E^T(\mathbf{x}, \mathbf{y}) K(\mathbf{x}, \mathbf{y}) E(\mathbf{x}, \mathbf{y}) \rangle_V, \quad (22)$$

$$\nabla_{\mathbf{y}} \cdot (K(\mathbf{x}, \mathbf{y}) E(\mathbf{x}, \mathbf{y})) = 0, \quad (23)$$

respectively (T indicates transpose). Moreover, by (18)

$$\nabla p_i^\epsilon = E \nabla p_i + \epsilon \nabla \theta_i^\epsilon + \dots, \quad (24)$$

where p_i is the homogenized solution given by

$$\nabla \cdot K^*(\mathbf{x}) \nabla p_i = 0 \quad \text{in } V, \quad p_i = x_i \quad \text{on } \partial V; \quad (25)$$

and θ_i^ϵ satisfies

$$\nabla \cdot K^\epsilon \nabla \theta_i^\epsilon = 0 \quad \text{in } V, \quad \theta_i^\epsilon = -\chi \cdot \nabla p_i \quad \text{on } \partial V. \quad (26)$$

From (13), (24) and (20) it can be shown that

$$\tilde{K}_{ij} = \langle (E \nabla p_i + \nabla \theta_i^\epsilon) \cdot K^\epsilon (E \nabla p_j + \nabla \theta_j^\epsilon) \rangle_V + O(\epsilon) \quad (27)$$

(see Appendix B). Expanding the integrand of (27) and using the symmetry of K^ϵ , we get

$$\begin{aligned} \tilde{K}_{ij} &= \langle (E \nabla p_i) \cdot K^\epsilon (E \nabla p_j) \rangle_V + 2\epsilon \langle (\nabla \theta_i^\epsilon) \cdot K^\epsilon (E \nabla p_j) \rangle_V \\ &\quad + \epsilon^2 \langle (\nabla \theta_i^\epsilon) \cdot K^\epsilon \nabla \theta_j^\epsilon \rangle_V + O(\epsilon). \end{aligned} \quad (28)$$

We estimate the two terms with θ_i^ϵ first. Due to the fact [14] that

$$\|\nabla \theta_i^\epsilon\|_V \leq Ch^{\frac{d-1}{2}} \epsilon^{-\frac{1}{2}} \quad (29)$$

and that the volume of V is $O(h^d)$, the last term is of order ϵ/h . For the second term, integration by parts gives

$$\int_V (\nabla \theta_i^\epsilon) \cdot K^\epsilon (E \nabla p_j) = \int_{\partial V} \theta_i^\epsilon \mathbf{n} \cdot (K^\epsilon E \nabla p_j) dS - \int_V \theta_i^\epsilon \nabla \cdot (K^\epsilon E \nabla p_j) dx \quad (30)$$

Since ∇p_j and E are bounded on ∂V in appropriate norms, the surface integral is bounded by $C\epsilon h^{d-1}$. For the volume integral on the right-hand side, noting that $\nabla = \nabla_{\mathbf{x}} + (1/\epsilon) \nabla_{\mathbf{y}}$ and using (23), we have

$$\nabla \cdot (K^\epsilon E \nabla p_i) = \nabla_{\mathbf{x}} \cdot (K(\mathbf{x}, \mathbf{y}) E(\mathbf{x}, \mathbf{y}) \nabla p_i) + (K^\epsilon E) : (\nabla \nabla p_i)$$

with ‘:’ indicating double contraction between tensors. By the estimates of $\|\theta_i^\epsilon\|_V$, $\|\nabla p_i\|_V$, and $\|p_i\|_{2,V}$ (see Appendix B), and the fact that K and E are smooth functions in \mathbf{x} , the volume integral is $O(\epsilon h^d)$. It follows that

$$\left| \tilde{K}_{ij} - \langle (E \nabla p_i) \cdot K^\epsilon (E \nabla p_j) \rangle_V \right| \leq C_1 \frac{\epsilon}{h} + C_2 \epsilon. \quad (31)$$

REMARK 1. *We would like to note that direct estimate of the l.h.s. of (30) using Cauchy-Shwartz inequality will yield $\sqrt{\epsilon/h}$ instead of ϵ/h in (31).*

Now, consider the first term in (28). Because

$$\langle (E \nabla p_i) \cdot K^\epsilon (E \nabla p_j) \rangle_V = \langle \nabla p_i \cdot (E^T K^\epsilon E) \nabla p_j \rangle_V,$$

from (22) and Lemma B.1 (Appendix B.2) we get

$$\langle (E \nabla p_i) \cdot K^\epsilon (E \nabla p_j) \rangle_V = \langle (\nabla p_i) \cdot K^*(\nabla p_j) \rangle_V + O\left(\frac{\epsilon}{h}\right). \quad (32)$$

Using (25) and integration by parts, we further have shown that

$$\langle (\nabla p_i) \cdot K^*(\nabla p_j) \rangle_V = \langle K_{ij}^* \rangle_V - \langle w_i \nabla \cdot (K_{ij}^* \mathbf{e}_j) \rangle_V,$$

where $w_i = p_i - x_i$. Thus, it follows from the Cauchy-Schwartz inequality and (46) that

$$\begin{aligned} \left| \langle (\nabla p_i) \cdot K^* (\nabla p_j) \rangle_V - \langle K_{ij}^* \rangle_V \right| &\leq C \frac{1}{V} \|w_i\|_V \|\nabla \cdot (K^* \mathbf{e}_j)\|_V \\ &\leq Ch. \end{aligned} \quad (33)$$

Therefore, (21) follows immediately from (31), (32), and (33). It should be noted that in the above derivation, we only require V to be a convex block with reasonable aspect ratios. Thus (3.10) applies to general unstructured meshes.

Using (21) we can derive the estimates for upscaled pressure and velocity solutions. Suppose \tilde{K} is computed on all grid blocks, we have a piecewise constant upscaled permeability field, which we still denote by \tilde{K} . Let \tilde{p} , $\tilde{\mathbf{u}}$ be the solutions of the upscaled flow equation

$$\tilde{\mathbf{u}} = \tilde{K} \nabla \tilde{p}, \quad \nabla \cdot \tilde{\mathbf{u}} = f \quad (34)$$

in Ω . For simplicity, we assume p and \tilde{p} equal zero on $\partial\Omega$. From (34) and (4) we have

$$\nabla \cdot \tilde{K} (\nabla p - \nabla \tilde{p}) = \nabla \cdot (\tilde{K} - K^*) \nabla p.$$

Since \tilde{K} is positive definite, multiplying both sides by $p - \tilde{p}$ and integration by parts yield

$$\|\nabla p - \nabla \tilde{p}\|_\Omega \leq C \|(\tilde{K} - K^*) \nabla p\|_\Omega \leq C_1 \frac{\epsilon}{h} + C_2 h + C_3 \epsilon. \quad (35)$$

For the last inequality, we have used (21) and the fact that $\|\nabla p\|_\Omega$ is bounded. As a result, we have

$$\begin{aligned} \|\mathbf{u} - \tilde{\mathbf{u}}\|_\Omega &\leq \|\tilde{K} (\nabla p - \nabla \tilde{p})\|_\Omega + \|(K^* - \tilde{K}) \nabla p\|_\Omega \\ &\leq C_1 \frac{\epsilon}{h} + C_2 h + C_3 \epsilon. \end{aligned} \quad (36)$$

Moreover, from (35) and the Poincaré inequality we get

$$\|p - \tilde{p}\|_\Omega \leq C_1 \frac{\epsilon}{h} + C_2 h + C_3 \epsilon. \quad (37)$$

Note that $\|p - p^\epsilon\|_\Omega \leq C\epsilon$ (cf. [18]). Thus by the triangle inequality

$$\|p^\epsilon - \tilde{p}\|_\Omega \leq C_1 \frac{\epsilon}{h} + C_2 h + C_3 \epsilon. \quad (38)$$

Unlike the pressure solutions, the homogenized velocity, \mathbf{u} , does not approximate \mathbf{u}^ϵ in the L_2 norm. Their L_2 norm difference is in fact $O(1)$. Similarly, $\tilde{\mathbf{u}}$ does not approximate \mathbf{u}^ϵ in the L_2 norm. In fact, we have $\langle \mathbf{u}^\epsilon - \mathbf{u} \rangle_V = O(\epsilon/h)$ for $V \subset \Omega$, which is consistent with (3). This estimate holds also for $\langle \mathbf{u}^\epsilon - \tilde{\mathbf{u}} \rangle_V$. Thus, the velocity solution of the upscaled equation approximates the volume average of the fine scale velocity in the grid-blocks as $\epsilon \rightarrow 0$. In comparison, the velocity computed from MsFEM approximates \mathbf{u}^ϵ [14, 8]. We note that the small scale fluctuations of \mathbf{u}^ϵ are often important in simulating transport phenomena in multiphase flows [13, 7].

3.3. Remarks. Several observations can be made from (21). First, (21) implies that we can obtain K^* at a given point by computing the limit of \tilde{K} as $\epsilon \rightarrow 0$ in a series of shrinking blocks containing the point. This is consistent with the general argument in Section 2.1. Moreover, if K^* is constant, the derivation of (33) indicates that the $O(h)$ error in (21) vanishes. An example is the case of pure periodic media described by $K^\epsilon(\mathbf{x}) = K(\mathbf{x}/\epsilon)$. In general, however, K^* contains large scale heterogeneity; (21) shows that the size of grid-blocks should be small in comparison. This explains the observation that local upscaling is usually preferred against global upscaling (cf. [6]).

As noted above, (21) is valid for $h \gg \epsilon$. If $h \ll \epsilon$, a different derivation would show that $|\tilde{K}_{ij} - \langle K_{ij}^\epsilon \rangle_V|$ is $O(h/\epsilon)$. Thus, for fixed ϵ , $\tilde{K} \rightarrow K^\epsilon$ as $h \rightarrow 0$, and therefore, the “upscaled” solution approximates the fine scale solution for $h \ll \epsilon$.

The $h \sim \epsilon$ case deserves further examination. It is seen that the error increases as h approaches ϵ . This scale “resonance” phenomenon is fundamental in upscaling. The derivation of (21) reveals two sources of the resonance effect. One is due to the first order corrector θ_i^ϵ , whose main role is to enforce the boundary conditions of p_i^ϵ on ∂V ; the other comes from the volume average of functions with ϵ -periodic small scales (see (32)).

The scale resonance is a direct consequence of the objective of upscaling, namely dividing a globally coupled fine scale problem into many *decoupled* local problems in the coarse grid blocks. The decoupling is achieved by *artificial* local boundary conditions imposed on ∂V , such as (7). As pointed out in [14], the optimum boundary condition would be the ones consistent with the fine scale oscillations of the differential operator, which are solely determined by $\chi(\mathbf{x}, \mathbf{x}/\epsilon)$ for the model problem. However, boundary conditions (7) and (9) are inconsistent with χ since they enforce non-oscillatory Dirichlet conditions on ∂V or part of it. The periodic condition (8), on the other hand, allows oscillations on ∂V ; however, the oscillations match those of χ only when h coincides with multiples of ϵ . Any mismatch on ∂V is to be corrected by θ_i^ϵ . It can be shown that the correction occurs in a thin layer with a thickness about $O(\epsilon)$ near ∂V [3]. This boundary layer yields large gradient of θ_i^ϵ near ∂V , which is the main cause of the $O(\epsilon/h)$ error in (31) (this was shown indirectly through the estimate of $\nabla \theta_i^\epsilon$ in Appendix B). In the interior of V , however, $\nabla \theta_i^\epsilon$ is much smaller. For more detailed analytical and numerical study of θ_i^ϵ , see e.g., [14, 12].

The accuracy of upscaling is also strongly influenced by the size of the sample based on which the average is taken. The sample size is given by the size of the grid blocks. Intuitively, for media with ϵ -periodic small scale, the perfect sample sizes are multiples of the period ϵ . Otherwise, error occurs due to the mismatch between the block size and the perfect sample size. Mathematically, the mismatch gives rise to $O(\epsilon h^{d-1})$ bound in Lemma B.1. This type of resonance is referred to as the “cell resonance”; it has been analyzed in detail in the context of multiscale finite element method [8]. Eq. (33) shows that the cell resonance error is $O(\epsilon/h)$ for the present upscaling formulation.

4. Over-sampling Method. It is possible to design numerical methods to remove the resonance error. An over-sampling technique has been developed by the authors to remove the resonance due to the boundary layer of θ_i^ϵ . It is shown to be very effective when used together with the multiscale finite element method [12]. This technique can be borrowed here to improve the upscaling of permeability. The idea is to use a larger sampling block $S \supset V$, such that the distance between ∂S and V

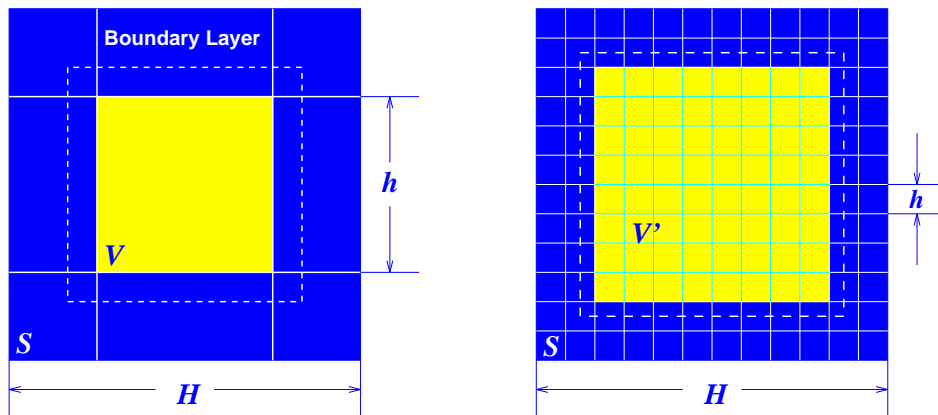


FIGURE 3. Over-sampling for one (left) and multiple (right) grid blocks. The boundary layer is outside the white dash line. V' denotes the union of the set of grid blocks in gray region.

is at least $O(\epsilon)$. Then we solve (5) in S and compute \tilde{K} using (2) in V . Since V is away from ∂S and is not “polluted” by the boundary layer of θ_i^ϵ , the resulting \tilde{K} is free from the resonance error due to θ_i^ϵ . The method is shown schematically in Fig. 3 (left). We further notice that the boundary conditions given in Section 2.2 may give different θ_i^ϵ . However, the main difference among these θ_i^ϵ s lie in the boundary layer region. Thus, by removing the boundary layers, different boundary conditions give rise to almost identical \tilde{K} . In other words, \tilde{K} depends mainly on K^ϵ and the partition of the domain.

We note that S can be as large as Ω . In fact, choosing large S that contains many grid blocks has the advantage of greatly reducing redundant calculations in the overlapping region near ∂S [12]. See the right figure in Fig. 3. In practice, however, it is difficult to use Ω as the sampling domain since the computation would be too expensive. Therefore, one may choose S as large as possible according to the computing resource. In a parallel implementation, S may be chosen so that the computation on S fits into the memory of each processor. In this way, the inter-processor communication is minimum.

Interestingly, in an attempt to reduce the effect of local boundary conditions, White and Horne [26] used the entire domain to sample fine scale solutions with different boundary conditions. The over-determined system of equation for \tilde{K} was solved by using the least square method. Inspired by their work, Gómez-Hernández [10] proposed a method of Laplacian with skin, where the width of the skin is arbitrarily set to half of the grid block size. Recently, Wen et al. [24] used one coarse grid ring around the coarse block to compute coarse grid permeabilities. The coarse permeability field is further used for two-phase flow simulations and the results are compared using one coarse ring with the results where no oversampling is performed. The authors obtained improved results using oversampling. More improvement has been observed for oriented and channeled permeability fields. These methods can now be analyzed and understood in the over-sampling framework.

It should be noted that the analysis in the previous section needs to be modified for the over-sampling method. Due to over-sampling, the equivalence between (2)

and (13) no longer holds. Thus, one needs to return to (2) for the computation of \tilde{K} and for the analysis of upscaling error. The basic ingredients of the analysis are the same as those given above. The main difference lies in θ_i^ϵ , whose gradient becomes smaller if oversampling is used [8]. In particular, it can be shown [8] that if $V \subset S$ is away from ∂S at least at a distance h , then we have

$$\|\nabla\theta_i^\epsilon\|_{L^\infty(V)} \leq \frac{C}{h}. \tag{39}$$

From (39) we have

$$\|\nabla\theta_i^\epsilon\|_{H^1(V)} \leq Ch^{d/2-1}.$$

Comparing this estimate to (29) we can conclude that the effect of θ_i^ϵ is reduced by using oversampling. We would like to note that the estimate (39) cannot be improved in general (see [18]). Although the estimate (39) is sharp, we have observed from numerical experiments that with the oversampling technique the computational error caused by the terms containing θ_i^ϵ is usually negligible.

The over-sampling is not helpful for reducing the cell resonance, which is governed by the grid block size. Therefore, the estimate (21) remains true even with the over-sampling. Nevertheless, below we demonstrate that numerically the error due to the cell resonance is small compared to that due to θ_i^ϵ . Thus, the over-sampling is still very effective in reducing the resonance error.

In comparison, the cell resonance error in the multiscale finite element method with over-sampling is $O(\epsilon^2/h^2)$ because of some additional error cancellation. Moreover, we found that by using linear test functions together with the multiscale base functions, the cell resonance can be removed completely.

5. Numerical Results. In this section, we provide some numerical results demonstrating the estimate (21) and the effect of over-sampling. For this purpose, we use a periodic K^ϵ without large scale heterogeneity. Thus, the $O(h)$ error in (21) vanishes, and we can focus on the resonance error. Tests with more general random permeability field are given in §5.2.

5.1. Periodic case. In the following, we compute the upscaled permeability \tilde{K} on one grid block $V = (0, 1)^2$ from

$$K^\epsilon(x, y) = 1/[2 + P \sin(2\pi(2x - y)/\epsilon)].$$

We fix $P = 1.8$. The exact effective permeability can be calculated analytically, we have

$$K_{11}^* = 0.62942, \quad K_{12}^* = K_{21}^* = 0.25883, \quad K_{22}^* = 1.01766.$$

We solve (5) with boundary conditions (7), (8), and (9) on uniform square grids using a Galerkin finite element method with bilinear base functions. \tilde{K} is computed from (2). For convenience, we denote \tilde{K}^i ($i = 1, 2, 3$) to be the numerical results obtained by using (7), (8), and (9), respectively.

First, we compute \tilde{K} with $\epsilon = 1$. In this case, the periodic condition (8) gives $\tilde{K} \equiv K^*$. The only error in this case is the discretization error. However, according to (21), using (7) and (9) gives rise to the resonance error. The error of \tilde{K}^1 and \tilde{K}^3 compared to K^* are presented in the next two tables, where N is the number of elements in the x and y directions. From the tables we see that the error in both cases does not converge to zero as grid refines. Evidently, the resonance error is dominating in these cases (note that $\epsilon/h = 1$); the error in the off-diagonal terms is especially large.

TABLE 1. Convergence of the numerical solution of \tilde{K}^1 to K^* ($\epsilon = h = 1$).

N	$ \tilde{K}_{11}^1 - K_{11}^* $	$ \tilde{K}_{12}^1 - K_{12}^* $	$ \tilde{K}_{21}^1 - K_{21}^* $	$ \tilde{K}_{22}^1 - K_{22}^* $
16	1.021e-1	1.229e-1	1.664e-1	2.095e-2
32	9.307e-2	1.130e-1	1.229e-1	1.564e-2
64	9.103e-2	1.107e-1	1.132e-1	1.439e-2
128	9.055e-2	1.101e-1	1.107e-1	1.408e-2

TABLE 2. Convergence of the numerical solution of \tilde{K}^3 to K^* ($\epsilon = h = 1$).

N	$ \tilde{K}_{11}^3 - K_{11}^* $	$ \tilde{K}_{12}^3 - K_{12}^* $	$ \tilde{K}_{21}^3 - K_{21}^* $	$ \tilde{K}_{22}^3 - K_{22}^* $
16	1.612e-2	2.001e-1	2.528e-1	5.278e-2
32	2.001e-2	1.961e-1	2.338e-1	5.615e-2
64	2.080e-2	1.951e-1	2.283e-1	5.690e-2
128	2.097e-2	1.949e-1	2.269e-1	5.708e-2

TABLE 3. Variation of $|\tilde{K}^1 - K^*|$ versus ϵ/h ($h = 1$).

N	ϵ	$ \tilde{K}_{11}^1 - K_{11}^* $	$ \tilde{K}_{12}^1 - K_{12}^* $	$ \tilde{K}_{21}^1 - K_{21}^* $	$ \tilde{K}_{22}^1 - K_{22}^* $
16	1.0	1.021e-1	1.229e-1	1.664e-1	2.095e-2
32	0.5	5.249e-2	6.358e-2	1.021e-1	1.297e-2
64	0.25	2.691e-2	3.299e-2	6.886e-2	8.843e-3
128	0.125	1.397e-2	1.752e-2	5.205e-2	6.754e-3
256	0.0625	7.474e-3	9.751e-3	4.360e-2	5.704e-3

As shown by (21), one way of reducing the resonance error is to reduce to ratio ϵ/h . This is demonstrated in Table 3 for \tilde{K}^1 . The result for \tilde{K}^3 is similar. The error of \tilde{K}_{11}^1 and \tilde{K}_{12}^1 decrease almost in the order of ϵ/h , but the error in \tilde{K}_{21}^1 and \tilde{K}_{22}^1 decrease more slowly. Note that the discretization error is fixed in the test because $N\epsilon$ is kept constant; hence, the error reduction is mainly due to the decrease of the resonance error (cf. (21)). Thus, faster error reduction can be seen for a component of \tilde{K} with more dominant resonance error. Numerically, we find that the resonance error is indeed much larger than the discretization error for \tilde{K}_{11}^1 and \tilde{K}_{12}^1 but not so for \tilde{K}_{21}^1 and \tilde{K}_{22}^1 .

The next table shows the improvement of resonance error due to over-sampling. The over-sampling method depicted in Fig. 3 is implemented. For convenience, we denote the distance between ∂S and V or V' by d_s . We take $\epsilon = 0.8$ in the tests. In this case, the over-sampling removes much but not all of the resonance error, because there is the cell resonance. We choose $S = (0, 4)^2$ and $V = (1, 3)^2$ at the center of S . Thus, $d_s = 1 > \epsilon$. The error of \tilde{K}_{21} and \tilde{K}_{22} are reported as they are larger than the error of the other two components. The results of using different upscaling boundary conditions appear to be quite similar, indicating that the influence of boundary conditions are small due to over-sampling. We note that in this particular test, the cell resonance is small as indicated by the decrease of error. Moreover, we note that (9) does give the correct off-diagonal terms of \tilde{K} if it is used correctly; otherwise, even the diagonal entries of \tilde{K} may be wrong.

TABLE 4. Resonance error reduction by over-sampling (N is the total number of elements in the x and y directions in S).

N	$ \tilde{K}_{12} - K_{12}^* $			$ \tilde{K}_{22} - K_{22}^* $		
	BC (7)	BC (8)	BC (9)	BC (7)	BC (8)	BC (9)
64	4.751e-2	4.748e-2	4.744e-2	9.953e-3	9.950e-3	1.018e-2
128	1.445e-2	1.443e-2	1.424e-2	1.952e-3	1.949e-3	2.203e-3
256	3.745e-3	3.725e-3	3.523e-3	4.771e-4	4.745e-4	7.351e-4

5.2. **Random cases.** Here, we present two tests of upscaling randomly generated permeability fields. The random field generator is based on the superposition of random modes in Fourier domain and fast Fourier transform to give K^ϵ in the physical domain. The details of the generator has been described in [12]. The purpose of these tests is to show that the difference in the upscaled permeability due to different upscaling boundary conditions can be effectively reduced by using the over-sampling. Thus, \tilde{K} depends solely on the geometry of the grid block and the underlying fine scale permeability.

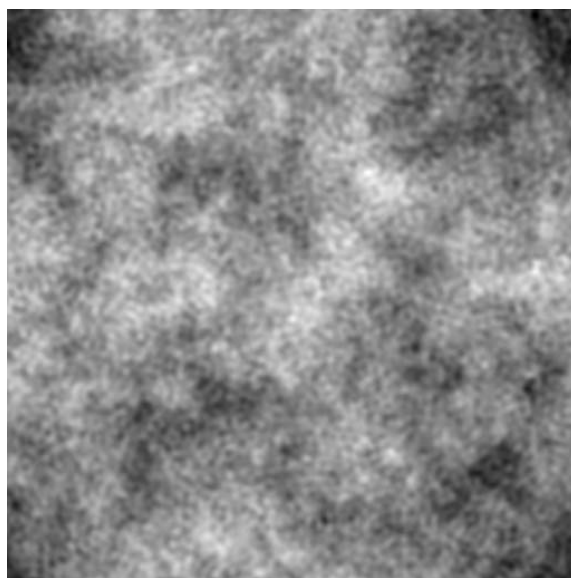
In these numerical tests, we compute the relative differences of \tilde{K} s. More specifically, we compute $D_{jk}^i = \|\tilde{K}_{jk}^i - \tilde{K}_{jk}^2\| / \|\tilde{K}_{jk}^2\|$ ($i = 1, 3$), where the norm is the discrete max or l_2 norm over Ω . The relative error of the solution of \tilde{p} is also checked against p^ϵ . For computing the pressure, we assume uniform injection $f = 1$ and $p = 0$ on $\partial\Omega$. The reference solution of p^ϵ is calculated from two fine-grid solutions using the Richardson extrapolation. The pressure error is denoted by E_p^i ($i = 1, 2, 3$), where i means the same as in \tilde{K}^i . For all tests below, uniform square mesh is used. Moreover, $\Omega = [0, 1]^2$, the permeability fields are generated on the 1024×1024 mesh, and the solutions of \tilde{K} and \tilde{p} are computed on the 32×32 coarse mesh. A 16×16 subcell mesh is used for upscaling of permeability.

In Case 1, a realization of a log-normal permeability field is generated. The highest wave number of the random modes used in generating the field is 32. The permeability field is in fact smooth and can be resolved by the 512×512 finite element mesh. It is scaled so that its contrast (i.e., $K_{max}^\epsilon / K_{min}^\epsilon$) is 400. In this case, the size of the grid blocks, $h = 1/32$, is about the correlation length of the permeability field (which often happens in practical simulations). Note that the correlation length is analogous to ϵ in the periodic case, we choose $d_s = h$ for the over-sampling. As shown by Table 5, our choice of d_s appears to be sufficiently wide for eliminating most of the effect of boundary conditions. Using smaller d_s , e.g., $h/2$, gives more error in \tilde{p}^1 and larger difference between \tilde{K}^1 and \tilde{K}^2 . In Table 5, only the diagonal entries of \tilde{K} are compared, because the off-diagonal entries are two orders of magnitude smaller than the diagonal ones and have much less effect on the pressure solution. Nevertheless, our numerical tests show that over-sampling has similar effect on the off-diagonal entries.

In some sense, the above problem is similar to the periodic problem because there is a distinctive small scale in permeability which is characterized by the correlation length. In practice, permeability distributions often exhibit multiple scales or no intrinsic small scale. In the next test, we use a permeability field whose logarithm has a fractal dimension of 2.8. The image of the field is shown in Fig. 4. In this case, how to choose d_s is not obvious; we determine it through the numerical experiment. The results for D^i and E_p^i are shown in Table 6. Two sets of over-sampling results

TABLE 5. Test of over-sampling using log-normal permeability Difference and error are shown in percentage.

	No Over-sampling		Over-sampling ($d_s = h$)	
	Max norm	l_2 norm	Max norm	l_2 norm
D_{11}^1	22.8125	17.2754	1.2233	0.5775
D_{11}^3	6.0135	2.8384	2.0317	0.5072
D_{22}^1	50.5283	18.3060	1.6727	0.6139
D_{22}^3	9.7429	2.9306	1.4441	0.4937
E_p^1	13.0553	12.7723	3.6848	1.6446
E_p^2	4.7253	2.2043	3.6459	1.6203
E_p^3	4.2316	2.0360	3.6182	1.6198

FIGURE 4. $\ln K^\epsilon$ with fractal dimension 2.8 (contrast of K^ϵ is 10^4).

are presented. We see that by using $d_s = 2h$, the difference between \tilde{K}^1 and \tilde{K}^2 and the error in the pressure solutions are reduced to the same level as in Table 5.

As mentioned in §4, over-sampling may lead to significant overhead in computations. In practice, such overhead can be greatly reduced by scale up many grid blocks together (Fig. 3). For the present computations, the sample domains are square regions containing 4×4 and 8×8 grid blocks for over-sampling with $d_s = h$ and $2h$, respectively. Note that due to the use of larger sample domain, the improved accuracy in the last column of Table 6 comes at no additional cost compared to the computation for the second column.

Interestingly, both Tables 5 and 6 show that the upscaling with the periodic and the pressure-drop no-flow boundary conditions (i.e., (9)) give very similar results. The pressure error using these boundary conditions are also quite small even without over-sampling. However, as indicated by the tests for the periodic problem,

TABLE 6. Test of over-sampling using permeability field shown in Fig. 4. Difference and error are shown in percentage.

	No Over-sampling		Over-sampling ($d_s = h$)		Over-sampling ($d_s = 2h$)	
	Max norm	l_2 norm	Max norm	l_2 norm	Max norm	l_2 norm
D_{11}^1	10.8141	7.3283	1.5048	1.2033	1.1942	0.7092
D_{11}^3	1.3060	1.0102	0.6799	0.4553	0.4875	0.2932
D_{22}^1	8.2273	7.4026	2.3588	1.6885	1.2986	0.7532
D_{22}^3	1.5108	1.0178	0.4657	0.4300	0.5565	0.4068
E_p^1	7.1424	6.5983	2.8717	1.7653	2.9171	1.4517
E_p^2	3.8179	1.5503	2.9465	1.3993	3.0436	1.3698
E_p^3	3.5359	1.5143	2.9519	1.3932	3.1065	1.3863

this is not always the case and should not be generalized. On the other hand, the use of the Dirichlet boundary condition (7) should always be accompanied by over-sampling. The advantage of (7) is that it is easy to apply on grid blocks with general geometry, i.e., those arisen from unstructured grids.

Appendix A. Formulation based on dissipation energy. Indelman and Dagan [15] suggested the use of averaged dissipation energy for determining the grid block permeability, i.e.,

$$\langle \nabla p \cdot \tilde{K} \nabla p \rangle_V = \langle \nabla p^\epsilon \cdot K^\epsilon \nabla p^\epsilon \rangle_V, \quad (40)$$

where p^ϵ is the solution of (5) and p is the solution of

$$\nabla \cdot \tilde{K} \nabla p = 0 \quad \text{in } V. \quad (41)$$

This formulation may be viewed as an approximation to the energy convergence in the homogenization theory (cf. [16]). Note that \tilde{K} cannot be uniquely determined from (40) since adding any anti-symmetric tensor to \tilde{K} does not change the equality. Thus, we enforce \tilde{K} to be symmetric.

Equation (40) is useful for calculating \tilde{K} only when ∇p is known in advance. This can be achieved by specifying special boundary conditions. Let $p = w + \mathbf{e} \cdot \mathbf{x}$ be the solution of (41), where \mathbf{e} is a constant vector. Then under the condition $w = 0$ on ∂V or w being periodic in V , we have $\nabla p = \mathbf{e}$ on V from (41) since \tilde{K} is a constant tensor in V . Thus (40) reduces to

$$\mathbf{e} \cdot \tilde{K} \mathbf{e} = \langle \nabla p^\epsilon \cdot K^\epsilon \nabla p^\epsilon \rangle_V. \quad (42)$$

This explicit formula is in fact equivalent to (13). We briefly outline the proof here.

First, because (42) holds for arbitrary \mathbf{e} , choosing $\mathbf{e} = \mathbf{e}_i$ ($i = 1, \dots, d$) and denoting the corresponding p^ϵ by p_i^ϵ , we obtain (13) for $i = j$. Now, choose $\mathbf{e} = \mathbf{e}_i + \mathbf{e}_j$ ($i \neq j$). By using the symmetry of \tilde{K} (as enforced) and K^ϵ , as well as the previous result for $i = j$, it is easy to show that (13) holds for $i \neq j$. On the other hand, since any vector \mathbf{e} can be written as a linear combination of \mathbf{e}_i , we obtain (42) from (13) by simple algebra. For this, we use the facts that (5) is linear and homogeneous, (7) (or (8)) is invariant under linear superposition, and that the two sides of (13) are bilinear forms.

With the boundary condition (9), $\nabla p = \mathbf{e}$ only when \tilde{K} is diagonal; otherwise, ∇p and \tilde{K} are coupled together and (40) could be difficult to use in actual computations.

We mention that reference [4] showed the above equivalence under the periodic boundary condition with a different approach, but the conclusion for the linear pressure drop condition (corresponding to $w = 0$ on ∂V) was incorrect.

Appendix B. Details of Derivations in Section 3.

B.1. **Derivation of (27).** Let

$$q_i^\epsilon = p_i + \epsilon \frac{\partial p_i}{\partial x_k} \chi^k + \epsilon \theta_i^\epsilon, \quad (43)$$

where p_i and θ_i^ϵ are given by (25) and (26), respectively. We need to show

$$\tilde{K}_{ij} = \langle \nabla p_i^\epsilon \cdot K^\epsilon \nabla p_j^\epsilon \rangle_V = \langle \nabla q_i^\epsilon \cdot K^\epsilon \nabla q_j^\epsilon \rangle_V + O(\epsilon). \quad (44)$$

Substituting $p_i^\epsilon = q_i^\epsilon + (p_i^\epsilon - q_i^\epsilon)$ into (13), we obtain the first term on the right-hand side of (44) and terms containing $p_i^\epsilon - q_i^\epsilon$. We prove the latter to be $O(\epsilon)$ below.

Let $p_i^\epsilon = x_i + w_i^\epsilon$ and $p_i = x_i + w_i$, the following estimates can be easily derived from (5) and (25):

$$\|\nabla w_i^\epsilon\|_V \leq Ch^{\frac{d}{2}}, \quad \|\nabla p_i^\epsilon\| \leq Ch^{\frac{d}{2}}; \quad (45)$$

$$\|w_i\|_V \leq Ch^{1+\frac{d}{2}}, \quad \|\nabla w_i\|_V \leq Ch^{\frac{d}{2}}, \quad \|\nabla p_i\|_V \leq Ch^{\frac{d}{2}}. \quad (46)$$

Furthermore, by elliptic regularity we have

$$\|p_i\|_{2,V} = \|w_i\|_{2,V} \leq C\|\nabla \cdot (K^* \mathbf{e}_i)\|_V \leq Ch^{\frac{d}{2}}. \quad (47)$$

For θ_i^ϵ we have (cf. [14])

$$\|\theta_i^\epsilon\|_V \leq Ch^{\frac{d}{2}}, \quad \|\nabla \theta_i^\epsilon\|_V \leq Ch^{\frac{d-1}{2}} \epsilon^{-\frac{1}{2}}.$$

It follows from (20) and (47) that

$$\|\nabla p_i^\epsilon - \nabla q_i^\epsilon\|_V \leq C\epsilon \|p_i\|_{2,V} \leq C\epsilon h^{\frac{d}{2}}. \quad (48)$$

Now (44) can be derived using (45) and (48). As an example, we have

$$\begin{aligned} \frac{1}{V} \int_V \nabla p_i^\epsilon \cdot K^\epsilon \nabla (p_j^\epsilon - q_j^\epsilon) d\mathbf{x} &\leq C \frac{1}{V} \|\nabla p_i^\epsilon\|_V \|\nabla (p_j^\epsilon - q_j^\epsilon)\|_V \\ &\leq Ch^{-d} h^{d/2} \epsilon h^{d/2} = C\epsilon. \end{aligned}$$

Other terms involving $p_i^\epsilon - q_i^\epsilon$ can be similarly estimated; they are $O(\epsilon)$.

B.2. An averaging lemma.

LEMMA B.1. *Given domain V with $\text{diam}(V) = h$, let $g(\mathbf{x}, \mathbf{y})$ be a Y -periodic function in \mathbf{y} , where Y is a unit cube. Assume $g(\mathbf{x}, \mathbf{y}) \in C^1(V) \cap C^0(Y)$. Then for any $f(\mathbf{x}) \in H^1(V) \cap C^0(\bar{V})$, we have*

$$\left| \int_V f(\mathbf{x}) g(\mathbf{x}, \mathbf{x}/\epsilon) d\mathbf{x} - \int_V f(\mathbf{x}) \langle g \rangle_Y(\mathbf{x}) d\mathbf{x} \right| \leq C\epsilon h^{d-1},$$

where

$$\langle g \rangle_Y(\mathbf{x}) = \frac{1}{Y} \int_Y g(\mathbf{x}, \mathbf{y}) d\mathbf{y}$$

is the average of g .

It suffice to prove for $\langle g \rangle_Y = 0$; otherwise we may consider $g - \langle g \rangle_Y$. The proof of a similar lemma with $g^\epsilon = g(\mathbf{x}/\epsilon)$ has been given in [8]. Using the lemma below, Lemma B.1 follows the proof of Lemma 3.2 in [8] with minor modifications.

LEMMA B.2. Let $g(\mathbf{x}, \mathbf{y})$ be defined in $V \times Y$ as above with $\langle g \rangle_Y = 0$ and $Y_\epsilon \subset V$ be a rescaled Y of size ϵ . We have

$$\left| \int_{Y_\epsilon} g(\mathbf{x}, \mathbf{x}/\epsilon) d\mathbf{x} \right| \leq C\epsilon^{d+1}.$$

Proof. Since $\langle g \rangle_Y = 0$, the Poisson equation

$$\Delta_{\mathbf{y}}\phi(\mathbf{x}, \mathbf{y}) = g(\mathbf{x}, \mathbf{y})$$

has a unique periodic solution ϕ with $\langle \phi \rangle_Y = 0$. Define $\boldsymbol{\xi} = \nabla_{\mathbf{y}}\phi$, we have $\nabla_{\mathbf{y}} \cdot \boldsymbol{\xi} = g$. Let $\mathbf{y} = \mathbf{x}/\epsilon$, we have $\nabla = \nabla_{\mathbf{x}} + (1/\epsilon)\nabla_{\mathbf{y}}$. Thus,

$$\begin{aligned} \int_{Y_\epsilon} g(\mathbf{x}, \mathbf{x}/\epsilon) d\mathbf{x} &= \int_{Y_\epsilon} \nabla_{\mathbf{y}} \cdot \boldsymbol{\xi}(\mathbf{x}, \mathbf{y}) d\mathbf{x} \\ &= \int_{Y_\epsilon} \epsilon(\nabla - \nabla_{\mathbf{x}}) \cdot \boldsymbol{\xi}(\mathbf{x}, \mathbf{y}) d\mathbf{x} \\ &= \epsilon \left(\int_{\partial Y_\epsilon} \mathbf{n} \cdot \boldsymbol{\xi}(\mathbf{x}, \frac{\mathbf{x}}{\epsilon}) dS - \int_{Y_\epsilon} \nabla_{\mathbf{x}} \cdot \boldsymbol{\xi}(\mathbf{x}, \mathbf{y}) d\mathbf{x} \right). \end{aligned} \tag{49}$$

The first term on the r.h.s. of the last equality can be written as

$$\sum_{i=1}^d \int_{\Gamma_i} [\xi_i(\mathbf{x} + \epsilon \mathbf{e}_i, \mathbf{y}) - \xi_i(\mathbf{x}, \mathbf{y})] dS,$$

where Γ_i is Y_ϵ 's face whose outward normal pointing to the \mathbf{e}_i direction. Note that we have used the periodicity of $\boldsymbol{\xi}$. By the smoothness assumption of g ,

$$|\xi_i(\mathbf{x} + \epsilon \mathbf{e}_i, \mathbf{y}) - \xi_i(\mathbf{x}, \mathbf{y})| \leq C\epsilon,$$

thus the surface integral in (49) is bounded by $C\epsilon^d$. Similarly, the last volume integral of (49) is bounded by $C\epsilon^d$. \square

Acknowledgments. The research was in part supported by a grant from National Science Foundation under the contract DMS-0073916, and by a grant from Army Research Office under the contract DAAD19-99-1-0141.

REFERENCES

- [1] J. Bear, "Dynamics of Fluids in Porous Media," Elsevier, 1972.
- [2] A. Bensoussan, J. L. Lions, and G. Papanicolaou, ASYMPTOTIC ANALYSIS FOR PERIODIC STRUCTURE, volume 5 of Studies in Mathematics and Its Applications, North-Holland Publ., 1978.
- [3] A. Bensoussan, J.-L. Lions, and G. Papanicolaou, BOUNDARY LAYER ANALYSIS IN HOMOGENEIZATION OF DIFFUSION EQUATIONS WITH DIRICHLET CONDITIONS IN THE HALF SPACE, Proceedings of the International Symposium on Stochastic Differential Equations (Res. Inst. Math. Sci., Kyoto Univ., Kyoto, 1976), pages 21–40, New York, 1978. Wiley.
- [4] O. Boe, ANALYSIS OF AN UPSCALING METHOD BASED ON CONSERVATION OF DISSIPATION, Transport in Porous Media, (1994), 77–86.
- [5] L. J. Durlofsky, NUMERICAL-CALCULATION OF EQUIVALENT GRID BLOCK PERMEABILITY TENSORS FOR HETEROGENEOUS POROUS MEDIA, Water Resour. Res., 27 (1991), 699–708.
- [6] L. J. Durlofsky, REPRESENTATION OF GRID BLOCK PERMEABILITY IN COARSE SCALE MODELS OF RANDOMLY HETEROGENEOUS POROUS-MEDIA, Water Resour. Res., 28 (1992), 1791–1800.
- [7] Y. R. Efendiev, L. J. Durlofsky, and S. H. Lee, MODELING OF SUBGRID EFFECTS IN COARSE SCALE SIMULATIONS OF TRANSPORT IN HETEROGENEOUS POROUS MEDIA, Water Resour. Res., 36 (2000), 2031–2041.
- [8] Y. R. Efendiev, T. Y. Hou, and X. H. Wu, THE CONVERGENCE OF NON-CONFORMING MULTI-SCALE FINITE ELEMENT METHODS, SIAM in Num. Anal., 37 (1999), 888–910.

- [9] L. C. Evans, "Weak convergence methods for nonlinear partial differential equations," Volume 74 of regional conference series in mathematics, AMS, Providence, R.I., 1990.
- [10] J. J. Gomez-Hernandez, "A stochastic approach to the simulation of block conductivity fields conditioned upon data measured at a smaller scale," Ph.D. thesis, Stanford University, 1991.
- [11] B. Hu, J. Cushman, and F.H. Deng, NONLOCAL REACTIVE TRANSPORT WITH PHYSICAL, CHEMICAL, AND BIOLOGICAL HETEROGENEITY, *Advances in Water Resources*, 20 (1997), 293–308.
- [12] T. Y. Hou and X. H. Wu, A MULTISCALE FINITE ELEMENT METHOD FOR ELLIPTIC PROBLEMS IN COMPOSITE MATERIALS AND POROUS MEDIA, *Journal of Computational Physics*, 134 (1997), 169–189.
- [13] T. Y. Hou and X. H. Wu, A MULTISCALE FINITE ELEMENT METHOD FOR PDES WITH OSCILLATORY COEFFICIENTS, *Numerical Treatment of Multi-Scale Problem*, *Notes Numer. Fluid Mech.* 70, pages 58–69. Vieweg-Verlag, 1999.
- [14] T. Y. Hou, X. H. Wu, and Z. Cai, CONVERGENCE OF A MULTISCALE FINITE ELEMENT METHOD FOR ELLIPTIC PROBLEMS WITH RAPIDLY OSCILLATING COEFFICIENTS, *Math. Comp.*, 68 (1999), 913–943.
- [15] P. Indelman and G. Dagan, UPSCALING OF PERMEABILITY OF ANISOTROPIC HETEROGENEOUS FORMATIONS I, *Water Resour. Res.*, 26 (1993), 917–923.
- [16] V. V. Jikov, S. M. Kozlov, and O. A. Oleinik, "Homogenization of differential operators and integral functionals," Springer-Verlag, 1994.
- [17] P. K. Kitanidis, EFFECTIVE HYDRAULIC CONDUCTIVITY FOR GRADUALLY VARYING FLOW, *Water Resour. Res.*, 26 (1990), 1197–1208.
- [18] Shari Moskow and Michael Vogelius, FIRST-ORDER CORRECTIONS TO THE HOMOGENISED EIGENVALUES OF A PERIODIC COMPOSITE MEDIUM. A CONVERGENCE PROOF, *Proc. Roy. Soc. Edinburgh Sect. A*, 127 (1997), 1263–1299.
- [19] Ph. Renard and G. de Marsily, CALCULATING EFFECTIVE PERMEABILITY: A REVIEW, *Advances in Water Resources*, 20 (1997), 253–278.
- [20] Y. Rubin and J.J. Gomez-Hernandez, A STOCHASTIC APPROACH TO THE PROBLEM OF UPSCALING OF CONDUCTIVITY IN DISORDERED MEDIA: THEORY AND UNCONDITIONAL NUMERICAL SIMULATIONS, *Water Resour. Res.*, 26 (1990), 691–701.
- [21] A. Saez, C. J. Otero, and I. Rusinek, THE EFFECTIVE HOMOGENEOUS BEHAVIOR OF HETEROGENEOUS MEDIA, *Transport in Porous Media*, (1989), 213–238.
- [22] R. E. Showalter and N. Su, PARTIALLY SATURATED FLOW IN A POROELASTIC MEDIUM, *Discrete and Continuous Dynamical Systems: Series B*, 1 (2001), 403–420.
- [23] X. H. Wen and J.J. Gomez-Hernandez, UPSCALING HYDRAULIC CONDUCTIVITIES IN HETEROGENEOUS MEDIA, *Journal of Hydrology*, 183 (1996), 9–32.
- [24] X.H. Wen, L.J. Durlofsky, S.H. Lee, and M.G Edwards, FULL TENSORUPSCALING OF GEOLOGICALLY COMPLEX RESERVOIR DESCRIPTIONS, SPE paper 62928, presented at the SPE Annual Technical Conference and Exhibition, Dallas, Oct. 1-4 (2000).
- [25] Mary F. Wheeler, Clint Dawson, and Joe Eaton, TRANSPORT OF MULTISPECIES CONTAMINANTS WITH BIOLOGICAL AND CHEMICAL KINETICS IN POROUS MEDIA, In "Modelling and computation for applications in mathematics, science, and engineering (Evanston, IL, 1996)," pages 25–37. Oxford Univ. Press, New York, 1998.
- [26] C. D. White and R. N. Horne, COMPUTING ABSOLUTE TRANSMISSIVITY IN THE PRESENCE OF FINE SCALE HETEROGENEITY, SPE, 16011 (1987), 209–221.

Received for publication January 2002.

E-mail address: x9wu1@upstream.xomcorp.com

E-mail address: efendiev@math.tamu.edu

E-mail address: hou@acm.caltech.edu